

NNLO QCD Corrections to  $t$ -channel Single Top-Quark Production and DecayEdmond L. Berger,<sup>1,\*</sup> Jun Gao,<sup>1,2,†</sup> C.-P. Yuan,<sup>3,‡</sup> and Hua Xing Zhu<sup>4,§</sup><sup>1</sup>*High Energy Physics Division, Argonne National Laboratory, Argonne, Illinois 60439, USA*<sup>2</sup>*Kavli Institute for Theoretical Physics, University of California, Santa Barbara, CA 93106, USA*<sup>3</sup>*Department of Physics and Astronomy, Michigan State University, East Lansing, Michigan 48824, USA*<sup>4</sup>*Center for Theoretical Physics, Massachusetts Institute of Technology, Cambridge, MA 02139, USA*

We present a fully differential next-to-next-to-leading order calculation of  $t$ -channel single top-quark production and decay at the LHC. We focus on the fiducial cross sections at 13 TeV, finding that the next-to-next-to-leading order QCD corrections can reach the level of  $-6\%$ . The scale variations are reduced to the level of a percent. Our results can be used to improve experimental acceptance estimates and the measurements of the single top-quark production cross section and the top-quark electroweak couplings.

**Introduction.** The top quark can be produced singly at a hadron collider through the electroweak (EW)  $Wtb$  vertex. There are three production channels: the  $t$ -channel and  $s$ -channel processes through exchange of a  $W$  boson, and associated production of  $tW$ . All three channels are sensitive to the structure of the  $Wtb$  vertex and to the CKM matrix element  $V_{tb}$ , an important motivation for their study. Moreover, single top production provides an important window to physics beyond the standard model (SM) [1], e.g., a modified  $Wtb$  vertex, new heavy quarks, new gauge bosons, flavor-changing neutral current, and so forth. Single top-quark production was first established at the Fermilab Tevatron [2, 3], and later at the Large Hadron Collider (LHC) [4–7]. Single top-quark studies are expected to enter an era of high precision during the upcoming run of the LHC at higher energy and larger luminosity.

The  $t$ -channel production has the largest rate among the three at the LHC, about 210 pb at  $\sqrt{s} = 13$  TeV. Significant efforts to improve the theoretical description of this process include next-to-leading order (NLO) QCD corrections in both 4- and 5-flavor schemes in Refs. [8–16]. Soft gluon resummation has been considered in Refs. [17–20]. Matching NLO calculations to parton showers is done in Refs. [21–23]. Recently, next-to-next-to-leading order (NNLO) QCD corrections with a *stable* top quark were calculated in Ref. [24], neglecting certain subleading contributions in color.

In this manuscript we present the first fully differential NNLO calculation of  $t$ -channel single top quark *production and decay* at the LHC in the 5-flavor scheme in QCD. We follow Ref. [24] in neglecting cross-talk between the hadronic systems of the two incoming protons. To the best of our knowledge, our calculation is the first to combine QCD corrections at NNLO for production and decay, meaning that a realistic simulation at NNLO is now available for leptonic top-quark decay in  $t$ -channel single top-quark production. The differential nature of our calculation allows us to impose phase space selections on final state objects, as done in the experiments (fiducial cuts). Using the fiducial cuts of the ATLAS and CMS analyses [25, 26], we find large NLO corrections, thus ne-

cessitating the higher order calculation performed here. The uncertainties associated with QCD hard-scale variation are reduced to the level of  $\sim 1\%$ . We compute the ratio of the top anti-quark to top quark production distributions with fiducial cuts applied, showing that sensitivity of this charge ratio to current parton distribution functions is much larger than to the perturbative corrections.

In the remaining paragraphs we outline the methods used in the calculation, and we present our numerical results on inclusive cross sections and fiducial cross sections and various differential distributions.

**Method.** We work in the Narrow-Width Approximation (NWA), under which the QCD corrections to the top-quark production and decay are factorizable. As confirmed by explicit numerical studies of off-shell and non-factorizable corrections [27, 28], this approximation is justified because the top-quark decay width is much smaller than its mass. We approximate the full QCD corrections by the *vertex* corrections; in the inclusive case, this is known as the structure function approach [29]. In this approach, we separate the QCD corrections into three factorizable contributions, as sketched in Fig. 1. There is a decay part  $V_d$ ; the light-quark line of the production part  $V_l$ ; and the heavy-quark line of the production part  $V_h$ . The use of the (fully differential) structure function approximation builds on the observation that QCD interference between the light-quark line and the heavy-quark line vanishes at NLO and is suppressed at least by a factor of  $1/N_c^2$  at NNLO. The use of such an approximation is also crucial for making this calculation feasible, because interference contributions between the light and heavy-quark lines are not yet available [30] for the full two-loop virtual diagrams. The structure function approximation at NNLO is also used in an earlier calculation of  $t$ -channel on-shell single top-quark production [24], and in Higgs boson production through weak boson fusion [31, 32].

The NNLO QCD corrections to the heavy-quark line are straightforward if we use phase-space slicing with the  $N$ -jettiness variable [33–35]. A similar calculation was

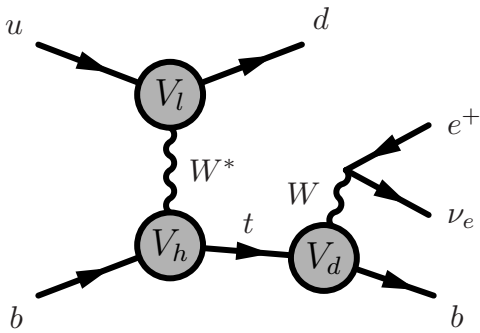


FIG. 1. Sketch of  $t$ -channel single-top quark production and decay;  $ub \rightarrow dt$  with  $t \rightarrow e^+ \nu_e b$ .  $V_l$  represents QCD corrections to the light quark line, which could include interference of the tree-diagram and the two-loop diagram, square of the one-loop diagram (double-virtual), interference of the one-loop diagram with one additional gluon and the tree-level diagram with one additional gluon (real-virtual), and the square of tree-level diagram with a pair of additional partons (double-real).  $V_h$  and  $V_d$  represent the same type of corrections to the heavy quark line and the decay part, respectively. There is no cross talk between the light quark line, heavy quark line, and the decay part in our calculation.

performed for charm quark production in neutrino deep inelastic scattering (DIS) in Ref. [36]. For the corrections to the light-quark line, we adopted the method of “projection-to-Born” in Ref. [32]. The key ingredients in this approach are the inclusive NNLO DIS coefficient functions [37–39], for which a conveniently parametrized version is available [40, 41]. For the real-virtual corrections, we extracted the one-loop helicity amplitudes from DIS 2 jet production in Ref. [42], and we cross checked with Gosam [43]. These ingredients were combined according to Ref. [32], by constructing appropriate counter-events with opposite weights for every event in the Monte Carlo (MC) integration of double-real and real-virtual contributions, which render the phase space integrals finite for infrared (IR) safe observables. For the decay part of the calculation, we adopted the results in Ref. [44]. We also take into account the product of two NLO corrections from different combinations of the light-quark line, the heavy-quark line, and the decay part.

Finally, we combine corrections to the production part and decay part consistently in the NWA, as in Refs. [45–47]. Schematically, we write

$$\begin{aligned}
 \sigma^{\text{LO}} &= \frac{1}{\Gamma_t^0} d\sigma^0 d\Gamma_t^0 \\
 \delta\sigma^{\text{NLO}} &= \frac{1}{\Gamma_t^0} \left[ d\sigma^1 d\Gamma_t^0 + d\sigma^0 (d\Gamma_t^1 - \frac{\Gamma_t^1}{\Gamma_t^0} d\Gamma_t^0) \right] \\
 \delta\sigma^{\text{NNLO}} &= \frac{1}{\Gamma_t^0} \left[ d\sigma^2 d\Gamma_t^0 + d\sigma^1 (d\Gamma_t^1 - \frac{\Gamma_t^1}{\Gamma_t^0} d\Gamma_t^0) \right. \\
 &\quad \left. + d\sigma^0 (d\Gamma_t^2 - \frac{\Gamma_t^2}{\Gamma_t^0} d\Gamma_t^0 - \frac{\Gamma_t^1}{\Gamma_t^0} (d\Gamma_t^1 - \frac{\Gamma_t^1}{\Gamma_t^0} d\Gamma_t^0)) \right], \quad (1)
 \end{aligned}$$

where  $d\sigma^i$  and  $d\Gamma_t^i$  denote the  $\mathcal{O}(\alpha_s^i)$  corrections to the production and decay parts, respectively. For the full NNLO corrections there are contributions from  $\mathcal{O}(\alpha_s^2)$  production only, from the product of  $\mathcal{O}(\alpha_s)$  production and  $\mathcal{O}(\alpha_s)$  decay, and from  $\mathcal{O}(\alpha_s^2)$  decay only, as shown in Eq. (1). Inclusive production cross sections at each order can be obtained after integration over the decay phase space.

**Numerical results.** We use a top quark mass of 173.2 GeV and a  $W$  boson mass of 80.385 GeV. We set the  $W$  boson decay branching ratio to 0.1086 for one lepton family. We choose  $|V_{tb}| = 1$  and the CT14 NNLO parton distribution functions (PDFs) [48] with  $\alpha_s(M_Z) = 0.118$ . The nominal scale choice is  $\mu_R = \mu_F = m_t$  with scale variation calculated by varying the two together over the range  $0.5 < \mu/\mu_o < 2$ . We list the LO, NLO and NNLO results for top quark and anti-quark production in Table. I. The NNLO QCD corrections reduce the cross sections by 2 ~ 3 % compared to a reduction of 4 ~ 5 % at NLO. The full NNLO corrections consist of pieces from the heavy-quark line, the light-quark line, and the products of them. There are cancellations between these pieces as well as cancellations among different partonic channels. Perturbative convergence of the separate QCD series is well maintained, as we verified by checking the individual pieces. Variations of the theoretical results associated with choices of the hard scales are reduced by a factor of 4 at NLO compared with LO, and by a further by a factor of 3 at NNLO with respect to NLO.

inclusive [pb]	LO	NLO	NNLO
$t$ quark	143.7 <sup>+8.1%</sup> <sub>-10%</sub>	138.0 <sup>+2.9%</sup> <sub>-1.7%</sub>	134.3 <sup>+1.0%</sup> <sub>-0.5%</sub>
$\bar{t}$ quark	85.8 <sup>+8.3%</sup> <sub>-10%</sub>	81.8 <sup>+3.0%</sup> <sub>-1.6%</sub>	79.3 <sup>+1.0%</sup> <sub>-0.6%</sub>

TABLE I. Inclusive cross sections for top (anti-)quark production at 13 TeV at various orders in QCD. The scale uncertainties are calculated by varying the hard scale from  $\mu_F = \mu_R = m_t/2$  to  $2m_t$ , and are shown in percentages.

Fiducial cross sections for  $t$ -channel single top-quark production have been measured at 7 and 8 TeV [25, 26]. We choose a fiducial region for 13 TeV that is similar to the one used in the CMS analysis [26] at 8 TeV. We use the anti- $k_T$  jet algorithm [49] with a distance parameter  $D = 0.5$ . Jets are defined to have transverse momentum  $p_T > 40$  GeV and pseudorapidity  $|\eta| < 5$ . We require exactly two jets in the final state, following the CMS and ATLAS analyses, meaning that events with additional jets are vetoed, and we require at least one of these to be a  $b$ -jet with  $|\eta| < 2.4$  [50, 51]. We demand the charged lepton to have a  $p_T$  greater than 30 GeV and rapidity  $|\eta| < 2.4$ . For the fiducial cross sections reported below we include top-quark decay to only one family of leptons.

Table II shows our predictions of the fiducial cross sec-

tions at different perturbative orders, with scale variations shown in percentages. We vary the renormalization and factorization scales  $\mu_R = \mu_F$  in the top-quark production stage, and the renormalization scale in the decay stage, independently by a factor of two around the nominal scale choice. The resulting scale variations are added in quadrature to obtain the numbers shown in Table II. We also show the QCD corrections from production and decay separately as defined in Eq. (1). All results shown in Table II are for the central scale choice  $m_t$ , as for the inclusive cross sections. The NNLO corrections from the product of  $\mathcal{O}(\alpha_s)$  production and  $\mathcal{O}(\alpha_s)$  decay can be derived by subtracting the above two contributions from the full NNLO corrections.

Changes of the QCD corrections after all kinematic cuts are applied are evident if one compares Table II with Table I. Acceptance in the charged lepton, the  $b$ -jet, and the non- $b$  jet produce these changes, as well as the jet veto. We call attention to the fact that the NLO QCD corrections in production have changed to  $-19\%$ . The NLO corrections in decay further reduce the cross sections by about 8%. At NNLO the correction in production is still dominant and can reach  $-6\%$ . The size of the NNLO correction in decay is smaller by about a factor of 2, and it almost cancels with the correction from the product of one-loop production and one-loop decay. Scale variations have been reduced to about  $\pm 1\%$  at NNLO. Scale variation bands at various orders do not overlap with each other in general.

fiducial [pb]		LO	NLO	NNLO
$t$ quark	total	$4.07^{+7.6\%}_{-9.8\%}$	$2.95^{+4.1\%}_{-2.2\%}$	$2.70^{+1.2\%}_{-0.7\%}$
	corr. in pro.		-0.79	-0.24
	corr. in dec.		-0.33	-0.13
$\bar{t}$ quark	total	$2.45^{+7.8\%}_{-10\%}$	$1.78^{+3.9\%}_{-2.0\%}$	$1.62^{+1.2\%}_{-0.8\%}$
	corr. in pro.		-0.46	-0.15
	corr. in dec.		-0.21	-0.08

TABLE II. Fiducial cross sections for top (anti-)quark production with decay at 13 TeV at various orders in QCD with a central scale choice of  $m_t$  in both production and decay. The scale uncertainties correspond to a quadratic sum of variations from scales in production and decay, and are shown in percentages. Corrections from pure production and decay are also shown.

With fiducial cuts applied, the jet veto introduces another hard scattering scale of  $p_{T,veto} = 40$  GeV in addition to  $m_t$ . Thus it may be appropriate to choose a QCD scale of  $(p_{T,veto}m_t)^{1/2} \sim m_t/2$ , especially at lower perturbative orders where the gluon splitting contributions are absorbed into the bottom-quark PDF. Alternative results with a central scale choice of  $m_t/2$  in production, with the central scale  $m_t$  retained in the decay part, show

better convergence of the series although the NNLO predictions are almost unchanged.

In experimental analyses, the total inclusive cross sections are usually determined through extrapolation of the fiducial cross sections based on acceptance estimates obtained from MC simulations. We can use the numbers shown in Tables I and II to derive the parton-level acceptance at various orders. For top quark production, the acceptances are 0.0283, 0.0214, and 0.0201 at LO, NLO, and NNLO respectively. The NNLO corrections can change the acceptance by 6% relative to the NLO value. This change also propagates into the measurement of the total inclusive cross section through extrapolation.

To compare our results with those in Ref. [24], we calculated the NNLO total inclusive cross sections at 8 TeV using the same choices of parameters. We found a difference of  $\sim 1\%$  on the NNLO cross sections. With a refined comparison through private communications, we traced the source of this discrepancy to NNLO contributions associated with  $V_h$ , with the  $b$ -quark initial state. All other parts in the NNLO corrections and all parts of the NLO contributions agree between the two results within numerical uncertainties. It has not been possible to further pin down the differences. We leave this issue for possible future investigation.

**Differential Distributions.** We present differential distributions for top quark production with decay. The effects for top anti-quark distributions are similar. The QCD corrections in production for the pseudorapidity distribution of the non- $b$  jet are shown in Fig. 2 after all fiducial cuts are applied. Events with two  $b$ -jets in the fiducial region are not included in the plot. The corrections depend strongly on the pseudorapidity. The NNLO corrections have a different shape from those at NLO and can be even larger than the NLO corrections in the regions of large pseudorapidity. The transverse momentum distribution of the leading  $b$ -jet is plotted in Fig. 3 with QCD corrections included only in the decay. The corrections reach a maximum for  $p_{T,b}$  of about 90 GeV. Acceptance limitations explain the peculiar shape of the distribution. We observe a reduction in the hard scale variations in both Figs. 2 and 3, calculated by varying the corresponding scales by a factor of two around  $m_t$ . The NNLO predictions are generally outside of the bands of the NLO scale variations.

Charge asymmetry is one of the precision observables at the LHC, e.g., as measured in  $W$  boson production [52–54]. It is insensitive to high-order corrections and is less subject to experimental systematic uncertainties. Moreover, since it is determined largely by the PDFs, it can provide stringent constraints in PDF determinations [48, 55]. The predicted ratio of the fiducial cross sections for top anti-quark and top quark production is presented in the upper panel of Fig. 4 as a function of the pseudorapidity of the charged lepton. The ratio

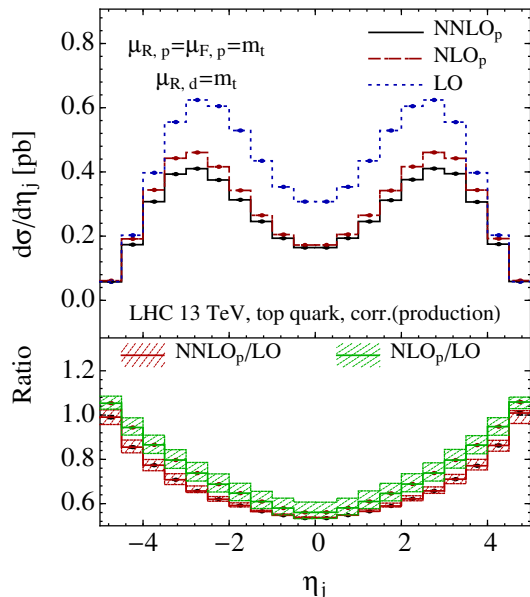


FIG. 2. Predicted pseudorapidity distribution of the non- $b$  jet in the final state from top quark production with decay at 13 TeV with fiducial cuts applied. Only QCD corrections in production are included.

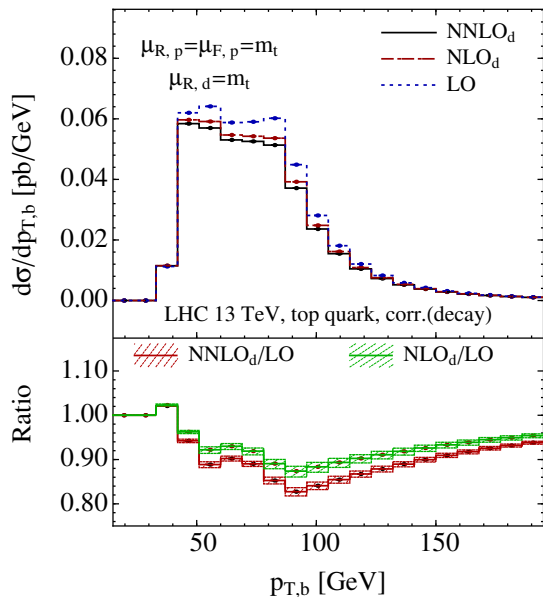


FIG. 3. Predicted transverse momentum distribution of the leading  $b$ -jet from top quark production with decay at 13 TeV with fiducial cuts applied. Only QCD corrections in decay are included.

is less than one since there are more  $u$ -valence quarks than  $d$ -valence quarks in the proton, and it decreases with pseudorapidity because the  $d/u$  ratio decreases at

large  $x$  [48]. The uncertainty flags show the statistical uncertainty from the MC integration. The ratios of the three curves are shown in the lower panel. The spread of the LO, NLO, and NNLO predictions is about 1% in the central region. At large  $|\eta_l|$ , the NLO correction can reach about 2%, and the additional NNLO correction is well below one percent. Also shown in the lower panel are the 68% confidence-level uncertainty bands for three sets of NNLO PDFs: CT14 [48], MMHT2014 [56] and NNPDF3.0 [57]. For simplicity, we obtained these bands using the LO matrix elements and the NNLO PDFs, and we verified that quantitatively similar central values of the bands are obtained if we use NLO matrix elements. Since the PDF induced uncertainty is much larger than the theoretical uncertainty of its NNLO prediction, the charge ratio can be used reliably to further discriminate among and constrain the PDFs, provided that experimental uncertainties can be controlled to the same level, as is also pointed out in [24]. This charge ratio may also be sensitive to certain kinds of physics beyond the SM [58].

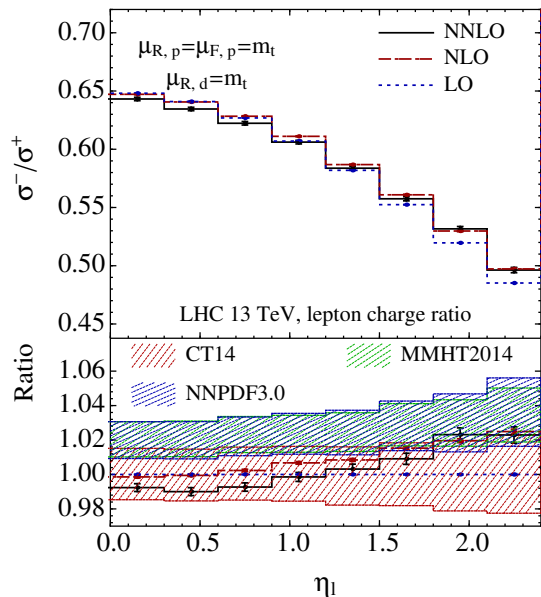


FIG. 4. Ratios of the fiducial cross sections of top anti-quark to top quark production with decay at 13 TeV as a function of the pseudorapidity of the charged lepton. The lower panel shows ratios to the LO prediction as well as dependence on the choice of PDFs.

**Summary.** We present the first calculation of NNLO QCD corrections to  $t$ -channel single top quark production with decay at the LHC in the 5-flavor scheme in QCD, neglecting the cross-talk between the hadronic systems of the two incoming protons. Our calculation provides a fully differential simulation at NNLO for  $t$ -channel single top-quark production with leptonic

decay at the parton level. The NNLO corrections reduce the scale uncertainties of the theoretical predictions to a percent level. For the kinematic cuts used in the 8 TeV LHC experimental analyses, the NNLO corrections to the fiducial cross sections can reach  $-6\%$ . Our results can be used to improve the determinations of the single top-quark production cross section and the top-quark electroweak coupling.

Work at ANL is supported in part by the U.S. Department of Energy under Contract No. DE-AC02-06CH11357. H.X.Z. was supported by the Office of Nuclear Physics of the U.S. DOE under Contract No. DE-SC0011090. This research was supported in part by the National Science Foundation under Grant No. NSF PHY-1125915 and PHY-1417326. We thank Ze Long Liu for cross-checking part of our results. We thank K. Melnikov and F. Caola for providing numbers on inclusive cross sections for crosschecks. We also thank T. Gehrmann, A. Papanastasiou, A. Signer, and Z. Sullivan for useful conversations. We thank Southern Methodist University for the use of the High Performance Computing facility ManeFrame.

---

\* berger@anl.gov

† jgao@anl.gov

‡ yuan@pa.msu.edu

§ zhuhx@mit.edu

- [1] T. M. P. Tait and C. P. Yuan, *Phys. Rev.* **D63**, 014018 (2000), hep-ph/0007298.
- [2] T. Aaltonen et al. (CDF), *Phys. Rev. Lett.* **103**, 092002 (2009), 0903.0885.
- [3] V. M. Abazov et al. (D0), *Phys. Rev. Lett.* **103**, 092001 (2009), 0903.0850.
- [4] G. Aad et al. (ATLAS), *Phys. Lett.* **B717**, 330 (2012), 1205.3130.
- [5] G. Aad et al. (ATLAS), *Phys. Lett.* **B716**, 142 (2012), 1205.5764.
- [6] S. Chatrchyan et al. (CMS), *JHEP* **12**, 035 (2012), 1209.4533.
- [7] S. Chatrchyan et al. (CMS), *Phys. Rev. Lett.* **110**, 022003 (2013), 1209.3489.
- [8] G. Bordes and B. van Eijk, *Nucl. Phys.* **B435**, 23 (1995).
- [9] R. Pittau, *Phys. Lett.* **B386**, 397 (1996), hep-ph/9603265.
- [10] T. Stelzer, Z. Sullivan, and S. Willenbrock, *Phys. Rev.* **D56**, 5919 (1997), hep-ph/9705398.
- [11] B. W. Harris, E. Laenen, L. Phaf, Z. Sullivan, and S. Weinzierl, *Phys. Rev.* **D66**, 054024 (2002), hep-ph/0207055.
- [12] Z. Sullivan, *Phys. Rev.* **D70**, 114012 (2004), hep-ph/0408049.
- [13] Q.-H. Cao, R. Schwienhorst, J. A. Benitez, R. Brock, and C. P. Yuan, *Phys. Rev.* **D72**, 094027 (2005), hep-ph/0504230.
- [14] J. M. Campbell, R. K. Ellis, and F. Tramontano, *Phys. Rev.* **D70**, 094012 (2004), hep-ph/0408158.
- [15] P. Falgari, P. Mellor, and A. Signer, *Phys. Rev.* **D82**, 054028 (2010), 1007.0893.
- [16] R. Schwienhorst, C. P. Yuan, C. Mueller, and Q.-H. Cao, *Phys. Rev.* **D83**, 034019 (2011), 1012.5132.
- [17] J. Wang, C. S. Li, H. X. Zhu, and J. J. Zhang (2010), 1010.4509.
- [18] N. Kidonakis, *Phys. Rev.* **D83**, 091503 (2011), 1103.2792.
- [19] J. Wang, C. S. Li, and H. X. Zhu, *Phys. Rev.* **D87**, 034030 (2013), 1210.7698.
- [20] N. Kidonakis (2015), 1510.06361.
- [21] S. Frixione, E. Laenen, P. Motylinski, and B. R. Webber, *JHEP* **03**, 092 (2006), hep-ph/0512250.
- [22] S. Alioli, P. Nason, C. Oleari, and E. Re, *JHEP* **09**, 111 (2009), [Erratum: *JHEP*02,011(2010)], 0907.4076.
- [23] R. Frederix, E. Re, and P. Torrielli, *JHEP* **09**, 130 (2012), 1207.5391.
- [24] M. Brucherseifer, F. Caola, and K. Melnikov, *Phys. Lett.* **B736**, 58 (2014), 1404.7116.
- [25] ATLAS-CONF-2014-007 (2014).
- [26] CMS-PAS-TOP-15-007 (2015).
- [27] P. Falgari, F. Giannuzzi, P. Mellor, and A. Signer, *Phys. Rev.* **D83**, 094013 (2011), 1102.5267.
- [28] A. S. Papanastasiou, R. Frederix, S. Frixione, V. Hirschi, and F. Maltoni, *Phys. Lett.* **B726**, 223 (2013), 1305.7088.
- [29] T. Han, G. Valencia, and S. Willenbrock, *Phys. Rev. Lett.* **69**, 3274 (1992), hep-ph/9206246.
- [30] M. Assadsolimani, P. Kant, B. Tausk, and P. Uwer, *Phys. Rev.* **D90**, 114024 (2014), 1409.3654.
- [31] P. Bolzoni, F. Maltoni, S.-O. Moch, and M. Zaro, *Phys. Rev. Lett.* **105**, 011801 (2010), 1003.4451.
- [32] M. Cacciari, F. A. Dreyer, A. Karlberg, G. P. Salam, and G. Zanderighi, *Phys. Rev. Lett.* **115**, 082002 (2015), 1506.02660.
- [33] I. W. Stewart, F. J. Tackmann, and W. J. Waalewijn, *Phys. Rev. Lett.* **105**, 092002 (2010), 1004.2489.
- [34] R. Boughezal, C. Focke, X. Liu, and F. Petriello, *Phys. Rev. Lett.* **115**, 062002 (2015), 1504.02131.
- [35] J. Gaunt, M. Stahlhofen, F. J. Tackmann, and J. R. Walsh, *JHEP* **09**, 058 (2015), 1505.04794.
- [36] E. L. Berger, J. Gao, C. S. Li, Z. L. Liu, and H. X. Zhu, *Phys. Rev. Lett.* **116**, 212002 (2016), 1601.05430.
- [37] W. L. van Neerven and E. B. Zijlstra, *Phys. Lett.* **B272**, 127 (1991).
- [38] E. B. Zijlstra and W. L. van Neerven, *Nucl. Phys.* **B383**, 525 (1992).
- [39] E. B. Zijlstra and W. L. van Neerven, *Phys. Lett.* **B297**, 377 (1992).
- [40] W. L. van Neerven and A. Vogt, *Nucl. Phys.* **B568**, 263 (2000), hep-ph/9907472.
- [41] W. L. van Neerven and A. Vogt, *Nucl. Phys.* **B588**, 345 (2000), hep-ph/0006154.
- [42] T. Gehrmann and E. W. N. Glover, *Phys. Lett.* **B676**, 146 (2009), 0904.2665.
- [43] G. Cullen et al., *Eur. Phys. J.* **C74**, 3001 (2014), 1404.7096.
- [44] J. Gao, C. S. Li, and H. X. Zhu, *Phys. Rev. Lett.* **110**, 042001 (2013), 1210.2808.
- [45] W. Bernreuther, A. Brandenburg, Z. G. Si, and P. Uwer, *Nucl. Phys.* **B690**, 81 (2004), hep-ph/0403035.
- [46] K. Melnikov and M. Schulze, *JHEP* **08**, 049 (2009), 0907.3090.
- [47] A. Broggio, A. S. Papanastasiou, and A. Signer, *JHEP*

- 10**, 98 (2014), 1407.2532.
- [48] S. Dulat, T.-J. Hou, J. Gao, M. Guzzi, J. Huston, P. Nadolsky, J. Pumplin, C. Schmidt, D. Stump, and C. P. Yuan, Phys. Rev. **D93**, 033006 (2016), 1506.07443.
- [49] M. Cacciari, G. P. Salam, and G. Soyez, JHEP **04**, 063 (2008), 0802.1189.
- [50] We define a parton-level  $b$ -jet as a clustered jet with non-zero bottom-quark number, e.g., a jet containing both a  $b$  quark and anti  $b$ -quark is not considered as a  $b$ -jet.
- [51] A. Banfi, G. P. Salam, and G. Zanderighi, Eur. Phys. J. **C47**, 113 (2006), hep-ph/0601139.
- [52] R. Aaij et al. (LHCb), JHEP **06**, 058 (2012), 1204.1620.
- [53] S. Chatrchyan et al. (CMS), Phys. Rev. **D90**, 032004 (2014), 1312.6283.
- [54] G. Aad et al. (ATLAS), Phys. Rev. **D85**, 072004 (2012), 1109.5141.
- [55] E. L. Berger, F. Halzen, C. S. Kim, and S. Willenbrock, Phys. Rev. **D40**, 83 (1989), [Erratum: Phys. Rev.D40,3789(1989)].
- [56] L. A. Harland-Lang, A. D. Martin, P. Motylinski, and R. S. Thorne, Eur. Phys. J. **C75**, 204 (2015), 1412.3989.
- [57] R. D. Ball et al. (NNPDF), JHEP **04**, 040 (2015), 1410.8849.
- [58] J. Gao, C. S. Li, L. L. Yang, and H. Zhang, Phys. Rev. Lett. **107**, 092002 (2011), 1104.4945.